photonics

MDPI

Communication

Performance Analysis of a Single Light Source Bidirectional Visible Light Communication Reverse Reflection Link

Ying Zhang [1,2,*], Jiawei Ren [1], Kexin Li [1] and Haibo Mou [1]

[1] School of Automation and Information Engineering, Xi'an University of Technology, Xi'an 710048, China; 2210320065@stu.xaut.edu.cn (J.R.); 2220321183@stu.xaut.edu.cn (K.L.); 2220320055@stu.xaut.edu.cn (H.M.)
[2] Xi'an Key Laboratory of Wireless Optical Communication and Network Research, Xi'an 710048, China
* Correspondence: zhangying@xaut.edu.cn

Abstract: Visible light communication has the advantages of large bandwidth, high security, and no RF interference, among which LED light sources are an important light source for indoor visible light communication. The use of LED as a light source for visible full-duplex communication is both to meet the lighting requirements and to ensure high-speed transmission of information. The uplink using the "cat's eye" reverse modulation system can greatly reduce the system complexity of the reverse reflector. In order to analyze the factors affecting the optical power at the receiving end of the uplink of the indoor single light source visible light communication, this paper establishes the indoor visible light full-duplex communication system model and deduces the calculation method of the effective incidence angle of the uplink transmission light and the movable range of the reverse reflection end according to the model. The results show that when the link distance of the BK7 lens is 3 m, the lens aperture is increased from 100 mm to 150 mm, the lens focal length is increased from 100 mm to 150 mm, the travel distance of the reverse reflector is increased by 60%, and the effective range of the incidence angle is increased by about twice. In the absence of link loss, each 1 m increase in link distance increases the maximum travel distance of the reverse reflector by 0.8 m. Increasing the lens aperture, decreasing the focal length, and increasing the link distance can improve the movable range of the reverse reflector, and the effective incidence angle changes more gently with the position of the reverse reflector.

Keywords: visible light communications; uplink; moving retroreflective end; effective incidence angle

check for updates

Citation: Zhang, Y.; Ren, J.; Li, K.; Mou, H. Performance Analysis of a Single Light Source Bidirectional Visible Light Communication Reverse Reflection Link. *Photonics* **2024**, *11*, 18. https://doi.org/10.3390/photonics11010018

Received: 7 November 2023
Revised: 3 December 2023
Accepted: 21 December 2023
Published: 26 December 2023

Copyright: © 2023 by the authors. Licensee MDPI, Basel, Switzerland. This article is an open access article distributed under the terms and conditions of the Creative Commons Attribution (CC BY) license (https://creativecommons.org/licenses/by/4.0/).

1. Introduction

Visible-light communication uses light as the transmission medium [1]. It has the two major advantages of high-speed optical communication and security in wireless communication and realizes the integration of lighting and communication at the same time. It has been listed as a new-generation communication technology [2,3].

Since visible light communication was proposed in 1999 [4], its transmission rate has been getting higher and higher, and it has continuously achieved breakthrough results. It has now reached 10 Gbps [5], but the uplink has always been a bottleneck inhibiting its development. Many studies focus on the form of uplink and propose solutions that integrate radio frequency WIFI [6–8], infrared [9], etc. with visible light. Heterogeneous links not only increase the complexity of the system but also limit the application of visible-light communication in certain scenarios. Vucic J et al. configured light sources at the terminal and built a time-division duplex visible light bidirectional link. By configuring the user time slot length, they improved the dynamic flexibility of asymmetric homogeneous link services [10]. However, the terminal's illumination [11,12] is not only detrimental to the mobility of the terminal but will also have a certain impact on indoor lighting. Using the principle of optical reflection to establish a reflection link based on cat's eye inverse modulation is an important technical means to achieve single-light source bidirectional

visible light communication [13,14]. It has the advantages of low power consumption, high security, low system structure complexity, and no electromagnetic interference [15]. Sun Y et al. analyzed the impact of the cat's eye inverse modulator structural parameters and link distance on the system's reflected light characteristics [16]. At present, research on reverse modulation visible light communication mainly solves problems such as the modulation format of the retroreflection signal and the suppression method of interference between links. To meet the high-speed, low-interruption, and other requirements for user hotspot high-capacity scenarios and small indoor scenarios [17], and to adapt to future 6G application development, the design of visible light communication systems needs to support mobility management and combine homogeneous uplinks. Road analysis of the impact of terminal mobility on the uplink is an important challenge in visible-light communication networking.

In this paper, based on the "cat's eye" reverse-modulated single-light source duplex communication uplink, we derive the relationship between the system parameters on the effective incidence angle and the effective movement of the reverse reflector. Therefore, we also establish a simulation model to verify the reliability of the formula. Through these, it is helpful to establish the uplink channel model of the single light source duplex visible light communication system so that the calculated optical power value of the uplink receiver is closer to the actual optical power value. Our work is summarized as follows:

(1) We established a single light source duplex visible light communication system model and derived the effective incidence angle of the light source that can reach the receiving end of the uplink and the maximum travel distance of the reverse reflector through geometric optics.
(2) In order to further verify the reliability of the formula, we establish a simulation model of the uplink of single-light source duplex visible light communication. Through simulation verification and formula derivation, we obtain the influence of the changes in system parameters on the effective incidence angle of the light source and the maximum travel distance of the reverse reflector.
(3) The effective incidence angle and the maximum travel distance of the reverse reflector represent the effective reflected light power of the system and the movement performance of the reverse reflector, respectively. The results show that increasing the lens aperture, decreasing the lens focal length, and increasing the link distance are conducive to increasing the moving range of the reverse reflector and maintaining the stability of the angle range of the incident light so as to stabilize the power reception at the receiving end.

The structure of this paper is arranged as follows: Section 2 introduces the structure of a reverse modulation system model based on "cat's eye". Section 3 introduces the formula derivation process based on system structure. Then, Section 4 analyzes the influence of system parameters on uplink performance based on Section 3. Section 5 establishes a simulation model to verify the reliability of the numerical analysis. Section 6 is the conclusion.

2. System Model

An equivalent model of the visible light retroreflection link consisting of an LED, convex lens, reflective surface, and detector is established, as shown in Figure 1. The light beam radiated by the LED converges to the reflective surface after passing through the modulation lens. The light beam reflected by the reflective surface passes through the modulation end lens and the receiving end lens and finally reaches the detector surface. The distance between the two lenses is L, the focal lengths of the receiving end and modulating end lenses are both f, and the vertical distance between the LED and the receiving end lens optical axis is H. If a certain light l_1 in the LED radiation beam reaches the modulating end lens input point A, the distance between this point and the optical axis of the lens is h, the angle between the light l_1 and the horizontal direction is α, and the angle between the light l_1 and the horizontal direction after exiting the modulation end lens is σ. Then the outgoing light after reflection by the reflecting surface is the angle between the horizontal direction is

β, and the longitudinal offset of the light spot formed by the reflected light l_2 after passing through the receiving end lens and reaching the detector is d.

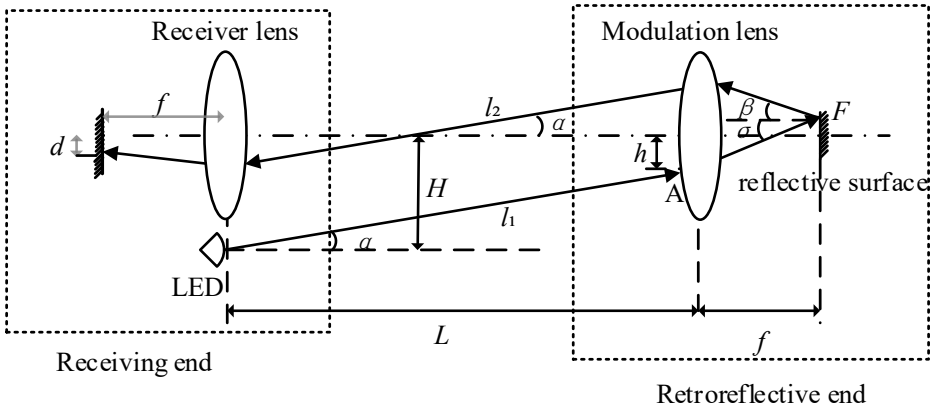

Figure 1. Uplink system model.

3. Retroreflective End Mobility Analysis

In a single-light source reverse visible light communication system, the optical power at the receiving end of the reflection link changes as the position of the retroreflective end changes, which will affect the optical power intensity at the receiving end, thereby affecting the efficiency of signal reception.

3.1. Lenses at Both Ends Are Coaxial

In the ideal optical system of the retroreflective link shown in Figure 1, the receiving end lens and the modulating end lens are coaxial, and the reflecting surface is at the focal plane of the convex lens. According to the thin lens theory, after parallel light passes through the optical system, it must intersect at a certain point on the focal plane of the image side. l_1 and l_2 are regarded as a group of rays entering the modulation lens and intersecting at point F on the focal plane. When, according to the law of reflection and the principle of the reversible optical path, the angle between l_1 and the optical axis is α, and the longitudinal offset is

$$d = f \times \tan \alpha \tag{1}$$

the offset of the light spot that reaches the detection surface after passing through the reverse modulation end will increase with the increase of α and f. According to the geometric relationship in the figure, we can know

$$\tan \alpha = \frac{H \pm h}{L} \tag{2}$$

among them, $\pm$ depends on the location of the light incident point. When the light incident point is above the optical axis of the reverse end lens, + is taken; otherwise, $-$is taken.

Substituting Formula (2) into Formula (1), we can get

$$d = \frac{H \pm h}{L} \times f \tag{3}$$

when other conditions remain unchanged, the spot offset distance d decreases with the increase of the link distance L and the distance h between the light incident point and the optical axis of the receiving end lens. As the distance H between the LED and the optical axis of the receiving end lens increases, the focal length increases.

By analyzing the characteristics of light transmission when coaxial, the angle of the reflected light cannot exceed the upper edge of the modulating lens. The light passing

through the modulating lens must be able to reach the receiving lens, so the following two conditions need to be met:

$$\begin{cases} 2f\tan\alpha < H - \frac{D}{2} \\ (\tan\alpha + \tan\beta)f \le \frac{D}{2} \end{cases} \tag{4}$$

in

$$\tan\beta = \tan\alpha + \frac{h}{f} \tag{5}$$

through Formula (4), we can get

$$\arctan\left(\frac{2H - D}{2(L - 2f)}\right) \le \alpha \le \arctan\left(\frac{2H + D}{4(L - f)}\right) \tag{6}$$

in the formula, D is the diameter of the lens.

According to the calculation formula for the luminous flux of the Lambertian light source, the effective luminous flux Φ reaching the retroreflective end lens can be obtained as

$$\Phi = \int_0^{2\pi} d\varphi \int_{\alpha_{\min}}^{\alpha_{\max}} I_0 \sin\alpha\cos\alpha d\alpha \tag{7}$$

in the formula, $\alpha_{\max}$ is the maximum incidence angle of the light source that can be received by the sending end; $\alpha_{\min}$ is the maximum incidence angle of the light source that can be received by the sending end.

Considering that the Lambertian light source has isotropic uniformity and its luminous intensity is I_0, we can get

$$\Phi = \pi I_0(\sin^2\alpha_{\max} - \sin^2\alpha_{\min}) \tag{8}$$

assuming that the reflection coefficient of the reflecting surface is m and the transmittances of the retroreflective end lens and the receiving end lens are both τ, then the luminous flux Φ' that can reach the receiving end lens is

$$\Phi' = m\tau\Phi \tag{9}$$

3.2. The Lenses at Both Ends Are Non-Coaxial

3.2.1. When the Optical Axis of the Modulation End Lens Moves Upward

It can be obtained from Figure 2.

$$\tan\alpha = \frac{H + s - h}{L} \tag{10}$$

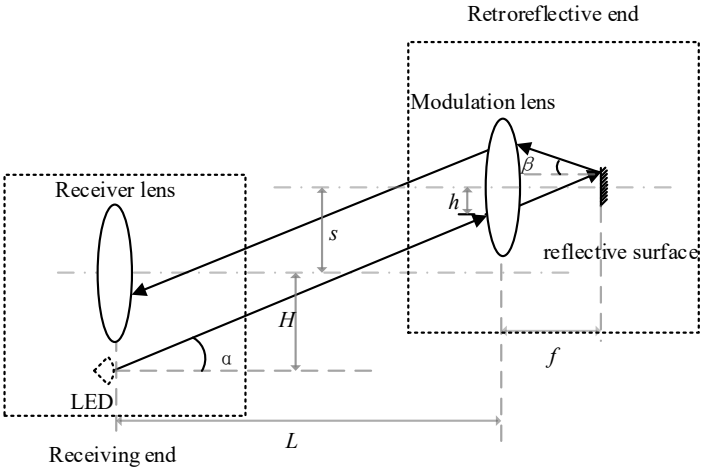

Figure 2. Schematic diagram of the upward movement of the retroreflective end.

According to the principle of optical path transmission, the value range of $\tan\alpha$ is

$$\frac{2H+4\mathrm{s}-\mathrm{D}}{4(L-f)} \leq \tan\alpha \leq \frac{2H+4s+D}{4(L-f)} \tag{11}$$

and

$$\tan\alpha \geq \frac{2H+2s-D}{2(L-2f)} \tag{12}$$

if the left part of Formula (11) is equal to the right part of Formula (12), because $D \leq 2H$, then we get $s = \frac{(D-2H)L}{8f} \leq 0$, therefore, by combining Formulas (11) and (12), we can get

$$\frac{2H+2s-D}{2(L-2f)} \leq \tan\alpha \leq \frac{2H+4s+D}{4(L-f)} \tag{13}$$

by substituting the value range of α obtained from Formula (13) into Formula (8), the optical power intensity value of the receiving end when the retroreflective end moves upward by a distance s can be obtained. When the equal sign in the above equation is established, that is

$$\frac{2H+2s-D}{2(L-2f)} = \frac{2H+4s+D}{4(L-f)} \tag{14}$$

from this, it can be obtained that the maximum range in which the retroreflective end can move upward is

$$s = \frac{3DL}{4f} - \frac{HL}{2f} - D \tag{15}$$

it can be seen from Formula (15) that the upward movable distance of the retroreflection end is related to the lens diameter D, the distance H between the light source and the receiving end lens optical axis, the lens focal length f, and the link distance L.

3.2.2. Modulation End Lens Moves Down

Figure 3 shows the situation when the retroreflective end moves downward along the vertical direction of the optical axis. It can be seen that:

$$\tan\alpha = \frac{H-s-h}{L} \tag{16}$$

when $\tan\alpha \geq 0$

$$\tan\alpha \geq \frac{2H-D-2s}{2(L-2f)} \tag{17}$$

and

$$\frac{2H-D-4s}{4(L-f)} \leq \tan\alpha \leq \frac{2H+D-4s}{4(L-f)} \tag{18}$$

by combining Formulas (17) and (18), we can get

$$\frac{2H-D-2s}{2(L-2f)} \leq \tan\alpha \leq \frac{2H+D-4s}{4(L-f)} \tag{19}$$

because $L-f>0$, when $2H+D-4s \geq 0$, so $H-\frac{D}{2} \leq s \leq \frac{H}{2}+\frac{D}{4}$, Formula (19) becomes

$$\frac{2H-2s-D}{2L} \leq \tan\alpha \leq \frac{2H+D-4s}{4(L-f)} \tag{20}$$

if $\tan\alpha \leq 0$, then $s > \frac{H}{2}+\frac{D}{4}$

$$\tan\alpha \geq \frac{2H-2s-D}{2L} \tag{21}$$

and

$$\frac{2H - D - 4s}{4(L - f)} \leq \tan\alpha \leq \frac{2H + D - 4s}{4(L - f)} \tag{22}$$

by combining Formulas (21) and (22), we can get

$$\frac{2H - 2s - D}{2L} \leq \tan\alpha \leq \frac{2H + D - 4s}{4(L - f)} \tag{23}$$

substituting the result obtained from Formula (23) into Formula (8), the optical power intensity value of the receiving end when the retroreflection end moves downward by a distance s will be obtained. When the equal sign is established, that is

$$\frac{2H - 2s - D}{2L} = \frac{2H + D - 4s}{4(L - f)} \tag{24}$$

the maximum distance that the reverse end moves downward can be obtained.

$$s = \frac{3LD}{4f} - \frac{LH}{2f} + H - \frac{D}{2} \tag{25}$$

combining Formulas (15) and (25), the maximum movable distance of the retroreflective end can be determined from the link distance L, lens focal length f, lens diameter D, and the distance H between the light source and the optical axis of the receiving end lens.

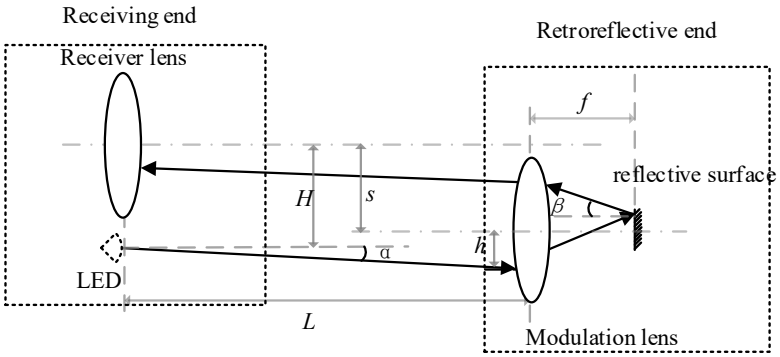

Figure 3. Schematic diagram of the retroreflective end moving downwards.

4. Numerical Analysis

To analyze the mobile performance of the reverse modulation end of the single-light source bidirectional visible light communication system and the factors affecting the mobile performance of the retroreflective end, assume that the distance H between the LED light source and the receiving end lens is 100 mm and the light source luminous power P is 1 W.

4.1. Retroreflective End Movable Range

Figure 4 shows the variation curve of the maximum moving distance of the retroreflective end with the link distance when the lens focal length is $f = 150$ mm. It can be seen from the figure that, under the same lens aperture parameters, there is a linear relationship between the maximum moving distance of the retroreflective end and the link distance. That is, the greater the link distance, the maximum movable distance of the retroreflective end also increases. The lens diameter also affects the maximum moving distance of the retroreflection end. The larger the lens diameter, the greater the slope of the change curve, indicating that the lens diameter has a greater impact on it.

When the lens diameter is $D = 100$ mm, the maximum moving distance of the retroreflection end changes with the link distance L, as shown in Figure 5. Under the same lens focal length, there is a linear relationship between the maximum moving distance of the retroreflective end and the link distance. That is, the greater the link distance, the greater the maximum distance the retroreflective end can move. The focal length of the

lens also affects the maximum moving distance of the retroreflective end. The smaller the focal length of the lens, the greater the slope of the change curve, which means that the focal length of the lens has a greater impact on it.

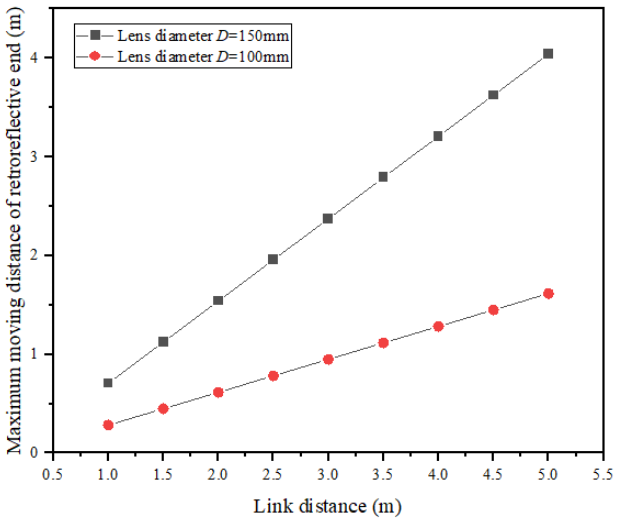

Figure 4. Variation curve of the maximum moving distance of the retroreflective end with the link distance *L*.

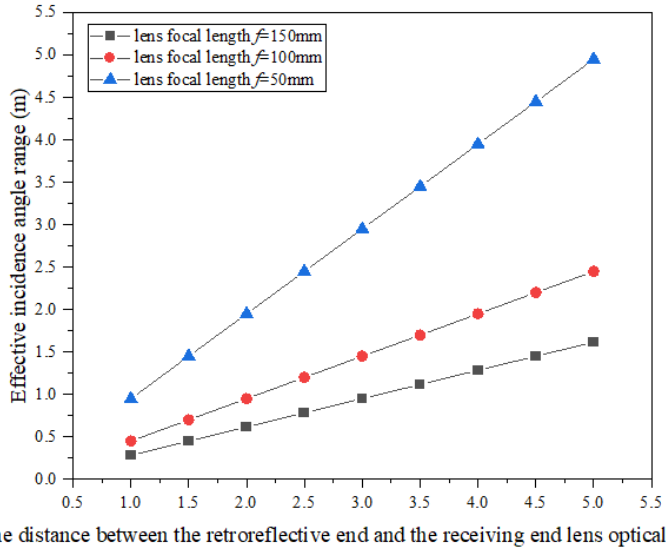

Figure 5. The variation curve of the maximum moving distance of the retroreflective end with the link distance *L* under different lens focal lengths *f*.

4.2. Effective Angle of Incidence

Under the conditions of lens focal length and lens diameter, the minimum incident angle and maximum incident angle of the light that can be received change as the retroreflective end moves, as shown in Figure 6. As the retroreflective end and the receiving end lens center light, the greater the distance between the axes, the greater the launch angle that can reach the receiving end, and the smaller the difference between the maximum incident angle and the minimum incident angle. As the link distance increases, the impact of the incident angle as the retroreflective end moves becomes smaller, the difference between the maximum incident angle and the minimum incident angle becomes smaller, and the movement range of the retroreflective end increases. Increasing the incident angle will lead to an increase in the offset of the light spot reaching the detector, so the larger the link distance, the smaller the

requirement for the detector area. Therefore, appropriately increasing the link distance will help increase the movement range of the retroreflective end.

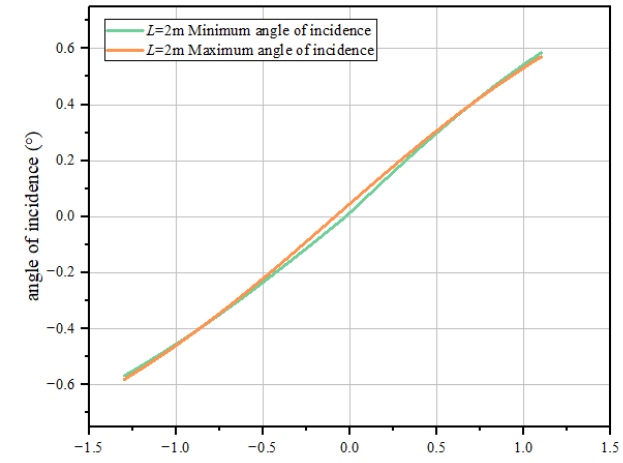

(**a**)

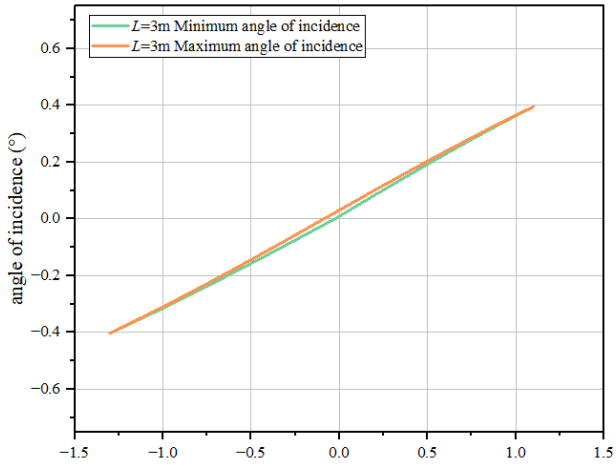

(**b**)

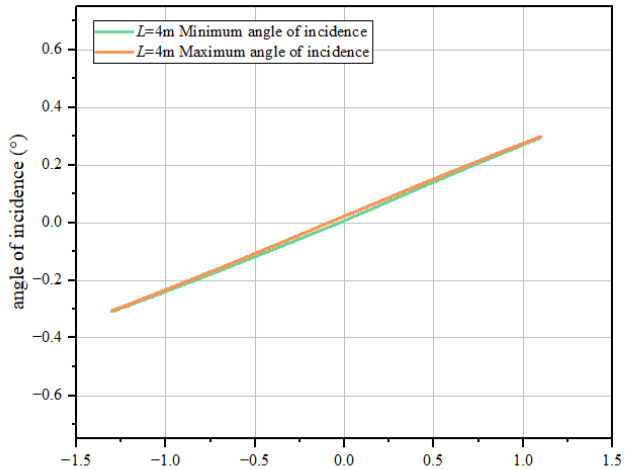

(**c**)

Figure 6. Under different link distances L, the change curve of the effective incident angle as the retroreflection end moves; (**a**) $L = 2\ m$; (**b**) $L = 3\ m$; (**c**) $L = 4\ m$.

Figure 7 is a graph showing the change of the effective incident angle range with the position of the retroreflection end under the conditions of link distance and lens focal length with different lens apertures. It can be seen from the figure that when the lens diameter is the same, the effective incident angle range will become smaller as the retroreflective end moves away from the central optical axis of the receiving lens. When the retroreflective end lens and the receiving end lens are coaxial, the effective incident angle range is the largest. For different lens diameters, the effective incident angle range changes with a similar trend as the retroreflection end changes. However, the larger the lens diameter, the greater the maximum value of the effective incident angle range.

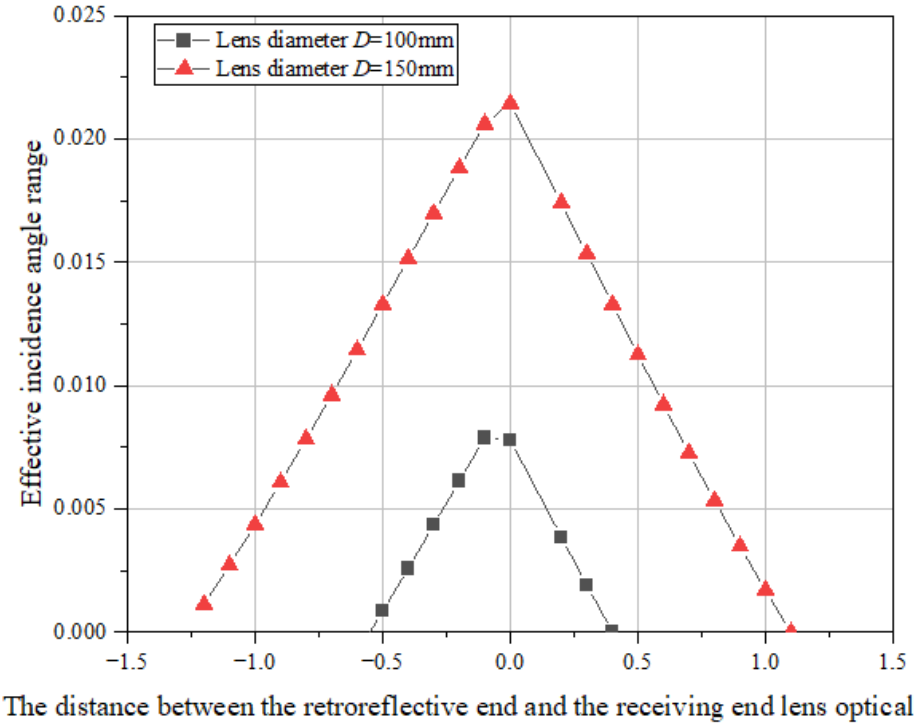

Figure 7. Variation curve of the effective incident angle range with the movement of the retroreflection end for different lens diameters.

Figure 8 is a graph showing the change of the effective incident angle range with the position of the retroreflection end under the conditions of link distance and lens focal length $D = 150$ mm, at different lens focal lengths. It can be seen that when the focal length of the lenses is the same when the retroreflective end lens is closer to the central axis of the receiving end lens, the effective incident angle range is the largest. For different lens focal lengths, the larger the lens focal length, the more obvious the change in the position of the retroreflection end in the effective reflection angle range. In practice, if the change in the effective reflection angle range can be reduced as much as possible within a large moving range, it will be beneficial to the receiving end in identifying the received signal. Therefore, a lens with a large aperture and a small focal length should be selected as a focus for visible light communication as much as possible.

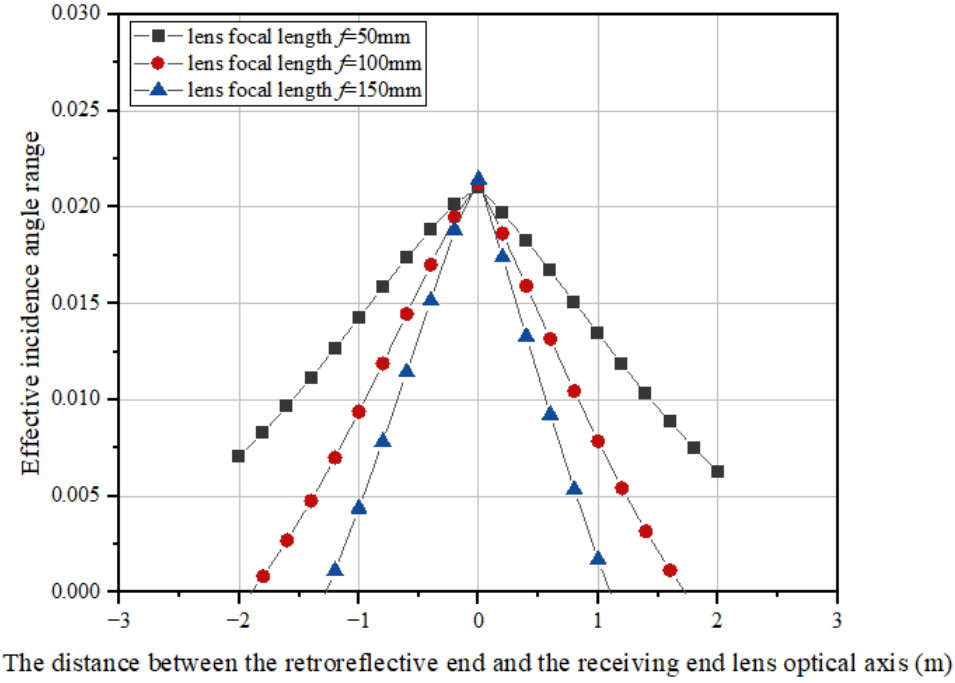

Figure 8. The effective incident angle range changes with the position of the retroreflection end when the lens focal length f is different.

5. Zemax Simulation Analysis

To further explore the factors affecting the visible light communication uplink, Zemax simulation software was used to verify the above results. The initial conditions set are shown in Table 1.

Table 1. Simulation initial conditions.

Parameter	Numerical Value
LED luminous power	1 W
LED divergence angle	60°
link distance	3 m
Distance between the LED and receiver lens	180 mm
lens material	BK7
Lens diameter	150 mm
lens focal length	150 mm

The data fitting curve of the maximum moving range of the retroreflection end as a function of the link distance L is shown in Figure 9. Under the same conditions as the simulation, the obtained results are consistent with the curve trend obtained by numerical calculation; that is, as the link distance increases, the maximum moving distance of the retroreflective end also increases. Since the simulation environment is close to the actual optical path of the lens, the maximum moving distance of the retroreflective end obtained through simulation shows a certain degree of nonlinearity.

Figure 10 shows the fitting curve of the maximum movable range of the retroreflective end as a function of the link distance at different lens apertures when other initial simulation conditions remain unchanged. Comparing Figure 4, we can see that there is a peak in the maximum moving range of the retroreflective end of the curve obtained by simulation, but the numerically calculated curve does not have this feature. This is because after the number of light rays set in the simulation reaches a certain distance, the light is too sparse, resulting in the reflection back. Less light is undetectable, so the maximum range of movement of the retroreflective end becomes smaller as the link distance increases. Before

the peak, the simulated fitting curve has the same trend as the curve obtained by numerical calculation, which further verifies the accuracy of the numerical calculation method.

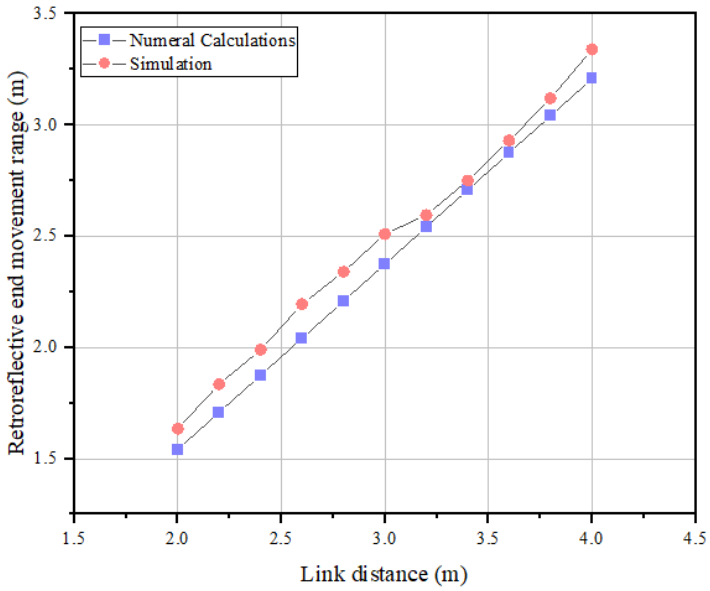

Figure 9. The curve of the movement range of the retroreflector as a function of link distance.

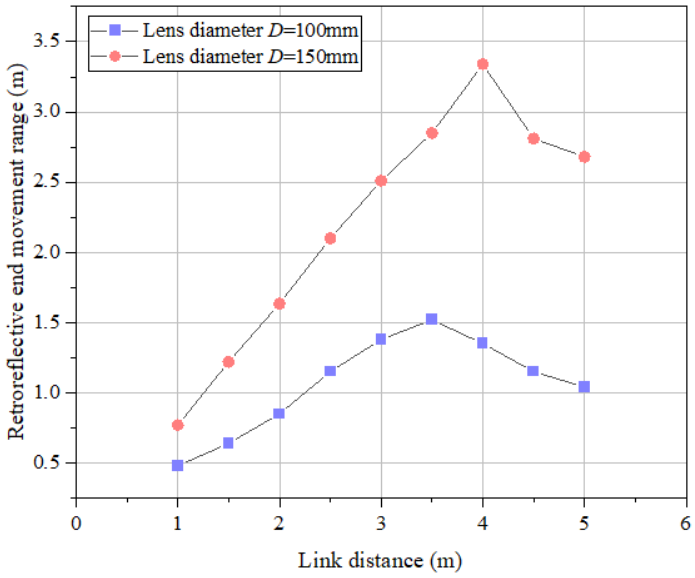

Figure 10. Simulation fitting curve of the maximum movable range of the retroreflective end changing with the link distance *L* for different lens diameters.

6. Conclusions

In this paper, the uplink model of single-light source duplex visible light communication is established. By establishing the "cat's eye" reverse modulation model, we mainly derive formulas based on geometric optics for the uplink of a single-light source duplex communication system and can clearly obtain the angle range of effective incident light when the reverse reflecting end is in a certain position. The maximum moving range of the reverse reflector at a certain link distance is obtained. Then, through the formula derived, it can be concluded that increasing the lens aperture, reducing the lens focal length, and increasing the link distance are conducive to increasing the moving range of the reverse reflector and maintaining the stability of the angle range of the incident light so as to stabilize the power reception at the receiving end. Finally, the simulation model of single-light source duplex visible light communication is established, and the simulation results are

consistent with the conclusions derived from the calculation. Based on this conclusion, this has a certain role in promoting the research of LED single light source duplex mobile communication and describes the channel characteristics more accurately so that the link between the communication parties is more stable and reliable.

Author Contributions: Conceptualization, Y.Z.; methodology, Y.Z. and J.R.; software, J.R.; validation, J.R., K.L., H.M. and Y.Z.; formal analysis, Y.Z.; investigation, J.R.; resources, Y.Z. and J.R.; data curation, Y.Z., K.L. and J.R.; writing—original draft preparation, Y.Z., H.M. and J.R.; writing—review and editing, Y.Z. and J.R. All authors have read and agreed to the published version of the manuscript.

Funding: This research was supported by the National Natural Science Foundation of China (61971345) and the Key Industrial Innovation Chain (Group)—Industrial Field Project of Shaanxi Province (2020ZDLGY05-02).

Institutional Review Board Statement: The study did not require ethical approval.

Informed Consent Statement: The study did not require ethical approval.

Data Availability Statement: The data that support the findings of this study are available from the corresponding author upon reasonable request.

Conflicts of Interest: The authors declare no conflicts of interest.

References

1. Koonen, T. Indoor Optical Wireless Systems: Technology, Trends, and Applications. *J. Light. Technol.* **2018**, *36*, 1459–1467. [CrossRef]
2. Feng, L.; Hu, R. Applying VLC in 5G networks: Architectures and key technologies. *IEEE Netw.* **2016**, *30*, 77–83. [CrossRef]
3. Jenila, C.; Jeyachitra, R. Green indoor optical wireless communication systems: Pathway towards pervasive deployment. *Digit. Commun. Netw.* **2021**, *7*, 410–444. [CrossRef]
4. Pang, G.; Kwan, T. Visible light communication for audio systems. *IEEE Trans. Consum. Electron.* **1999**, *45*, 1112–1118. [CrossRef]
5. Tanaka, Y. Wireless optical transmissions with white colored LED for wireless home links. In Proceedings of the 11th IEEE International Symposium on Personal Indoor and Mobile Radio Communications, PIMRC 2000, London, UK, 18–21 September 2000.
6. Ayyash, M. Coexistence of WiFi and LiFi toward 5G: Concepts, opportunities, and challenges. *IEEE Commun. Mag.* **2016**, *54*, 64–71. [CrossRef]
7. Ilker, D.; Daniel, C. Powering the Internet of Things through Light Communication. *IEEE Commun. Mag.* **2019**, *57*, 107–113.
8. Liu, X.; Huang, S. Joint Resource Allocation and Drones Relay Selection for Large-Scale D2D Communication Underlaying Hybrid VLC/RF IoT Systems. *Drones* **2023**, *7*, 589. [CrossRef]
9. Dhivya, G.; Hariharan, K.; Poonguzhali, P. ILLUMINATE-Visible Light Communication enabled Smart Indoor lighting and control System. In Proceedings of the 2023 25th International Conference on Advanced Communication Technology (ICACT), Pyeongchang, Republic of Korea, 19–22 February 2023.
10. Zhang, C.; Ge, J.; Pan, M. One Stone Two Birds: A Joint Thing and Relay Selection for Diverse IoT Networks. *IEEE Trans. Veh. Technol.* **2018**, *67*, 5424–54348. [CrossRef]
11. Ariyanti, S. Visible Light Communication (VLC) for 6G Technology: The Potency and Research Challenges. In Proceedings of the 2020 Fourth World Conference on Smart Trends in Systems, Security and Sustainability, London, UK, 27–28 July 2020.
12. Rui, B.; Iman, T.; Harald, H. 15.73 Gb/s Visible Light Communication with Off-the-Shelf LEDs. *J. Light. Technol.* **2019**, *37*, 2418–2424.
13. Chellam, J.; Jeyachitra, R.K. Energy-efficient bi-directional visible light communication using thin-film corner cube retroreflector for self-sustainable IoT. *IET Optoelectron.* **2020**, *14*, 223–233. [CrossRef]
14. Shao, S.; Salustri, A.; Khreishah, A. R-VLCP: Channel Modeling and Simulation in Retroreflective Visible Light Communication and Positioning Systems. *IEEE Internet Things J.* **2023**, *10*, 11429–11439. [CrossRef]
15. Khan, L. Visible Light Communication: Applications, Architecture, Standardization and Research Challenges. *Digit. Commun. Netw.* **2017**, *3*, 78–88. [CrossRef]
16. Sun, Y.; Ke, X. Analysis of factors affecting the characteristics of reverse modulated reflected light. *Infrared Laser Eng.* **2016**, *45*, 222–228.
17. Wang, L.; Han, D. Deep reinforcement learning-based adaptive handover mechanism for VLC in a hybrid 6G network architecture. *IEEE Access* **2021**, *9*, 87241–87250. [CrossRef]

Disclaimer/Publisher's Note: The statements, opinions and data contained in all publications are solely those of the individual author(s) and contributor(s) and not of MDPI and/or the editor(s). MDPI and/or the editor(s) disclaim responsibility for any injury to people or property resulting from any ideas, methods, instructions or products referred to in the content.